Published for SISSA by Springer

Received: *January 20, 2016*
Revised: *March 16, 2016*
Accepted: *April 11, 2016*
Published: *May 2, 2016*

How resonance-continuum interference changes 750 GeV diphoton excess: signal enhancement and peak shift

Sunghoon Jung,[a] **Jeonghyeon Song**[b] **and Yeo Woong Yoon**[b,c]

[a] *SLAC National Accelerator Laboratory, Menlo Park, CA 94025, U.S.A.*
[b] *School of Physics, KonKuk University, Seoul 143-701, Korea*
[c] *Korea Institute for Advanced Study, Seoul 130-722, Korea*

E-mail: shjung@slac.stanford.edu, jeonghyeon.song@gmail.com, ywyoon@kias.re.kr

Abstract: A hypothetical new scalar resonance, a candidate explanation for the recently observed 750 GeV diphoton excess at the LHC 13 TeV, necessarily interferes with the continuum background $gg \to \gamma\gamma$. The interference has two considerable effects: (1) enhancing or suppressing diphoton signal rate due to the imaginary-part interference and (2) distorting resonance shape due to the real-part interference. We study them based on the best-fit analysis of two benchmark models: two Higgs doublets with ∼50 GeV width (exhibiting the imaginary-part interference effect) and a singlet scalar with 5 GeV width (exhibiting the real-part one), both extended with vector-like fermions. We find that the resonance contribution can be enhanced by a factor of 2 (1.6) for 3 (6) fb signal rate, or the 68% CL allowed mass region is shifted by $\mathcal{O}(1)$ GeV. If the best-fit excess rate decreases in the future data, the interference effects will become more significant.

Keywords: Beyond Standard Model, Higgs Physics, Scattering Amplitudes

ArXiv ePrint: 1601.00006

doi:10.1007/JHEP05(2016)009

JHEP05(2016)009

Contents

JHEP05(2016)009

1 Introduction

Recently, mild excesses in diphoton invariant mass distribution have been observed in both ATLAS [1] and CMS [2] experiments at Large Hadron Collider (LHC) 13 TeV running. The local significances of the excesses are 3.6σ and 2.6σ, respectively, preferring a new resonance at around 750 GeV decaying to diphotons [1–3]. Although LHC 8 TeV data did not reveal significant excess at the same mass range, they are not currently inconsistent with the 13 TeV excess; see e.g. [3]. The tantalizing hint of a new resonance triggered various theoretical proposals [4–86] that are allegedly said to fit the 750 GeV excess rate $\sim \mathcal{O}(1)$ fb. Also, both a narrow and a somewhat broad resonance with $\Gamma \sim \mathcal{O}(10)$ GeV were found to fit the data similarly well [1, 3].

If a new scalar resonance contributes to the diphoton excess in the $gg \to \gamma\gamma$ channel, it necessarily interferes with the continuum $gg \to \gamma\gamma$ [87–94]. The interference, however, has been ignored in previous diphoton excess studies so far. The interference can have two considerable effects (see, e.g. ref. [93]):

(i) Enhancing or suppressing diphoton signal rate,

(ii) Distorting resonance shape.

The effects can be especially sizable if the resonance width is at least comparable to experimental resolutions or bin sizes, $\Gamma \gtrsim 5$ GeV. For the 125 GeV SM Higgs boson, for example, even though it is narrow, the resulting peak-shift is ~ 70 MeV [89, 91] and will be comparable to the pole-mass measurement uncertainty soon (currently ~ 490 MeV [95]). For

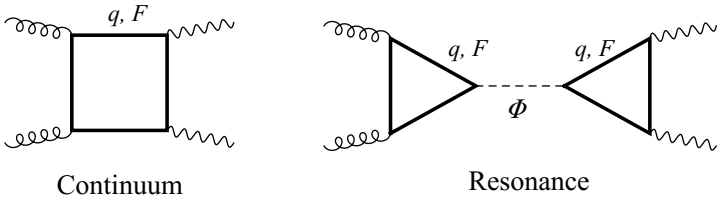

Figure 1. Representative Feynman diagrams of the interfering continuum background (left) and a scalar resonance signal (right) in the $gg \to \gamma\gamma$.

a 750 GeV gg-fused scalar resonance with $\mathcal{O}(1)$ fb diphoton rate, the resonance-continuum interference is generally large: the resonance-squared $S \sim \mathcal{O}(1)$ fb and the $gg \to \gamma\gamma$ continuum background $B \sim 0.2\,\text{fb}/40\,\text{GeV}$ naively generate $2\sqrt{SB}/S \sim (30-90)\%$ relative interference effect. The interference is particularly large in the diphoton channel because the scalar resonance contribution is two-loop while the interfering continuum background is only one-loop as shown in figure 1, so that the above naive estimation of the relative interference is generally loop-factor enhanced [93, 94].

The two main interference effects arise according to the relative phase between the resonance and the continuum processes. The real-part interference (with the relative phase $\phi \sim 0, \pi$, as will be defined and discussed) induces either peak-dip or dip-peak pattern added to a resonance peak, distorting the resonance shape from a pure resonance peak. On the other hand, the imaginary-part interference (with $\phi \sim \pi/2, 3\pi/2$) simply rescales the resonance peak, hence enhancing or suppressing the resonance peak. The non-zero phase is generated when some particles running in loops are lighter than 375 GeV.

In this paper, we investigate each interference effect on the current 750 GeV excess data by considering two benchmark models. Each model exhibits each interference effect. We first describe our method of calculating resonance shapes including interferences in section 2.1 and the diphoton datasets and best-fit analysis method in section 2.2. The two benchmark models are introduced and our main results are discussed in section 3 and section 4. Then we conclude and discuss prospects in section 5.

2 Formalism and analysis method

2.1 Diphoton rate and resonance shape

We consider a scalar resonance in the $gg \to \gamma\gamma$. It interferes with the one-loop continuum backgrounds shown in figure 1. The total differential cross section including the interference is written as

$$\begin{aligned}\frac{d\sigma}{dm_{\gamma\gamma}} &= \frac{d\sigma_{\text{cont}}}{dm_{\gamma\gamma}} + \frac{d\sigma_{\text{sig}}}{dm_{\gamma\gamma}} \\ &= \frac{2}{m_{\gamma\gamma}}\,\mathcal{L}_{gg}\left(\frac{m_{\gamma\gamma}^2}{s}\right)\left[\hat{\sigma}_{\text{cont}}(m_{\gamma\gamma}^2) + \hat{\sigma}_{\text{sig}}(m_{\gamma\gamma}^2)\right],\end{aligned} \tag{2.1}$$

JHEP05(2016)009

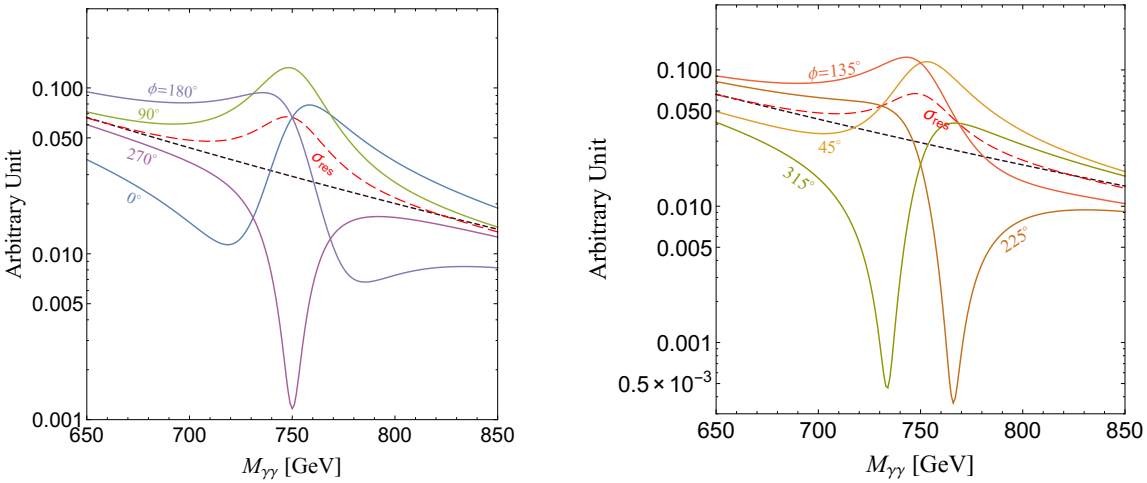

Figure 2. (*Left*): invariant mass distributions $\sigma(pp \to \Phi \to \gamma\gamma)$ at the 13 TeV LHC for the purely real-part ($\phi = 0, 180°$) and the purely imaginary-part ($\phi = 90°, 270°$) interference. (*Right*): invariant mass distributions for $\phi = 45°, 135°, 225°, 315°$. We set $M = 750\,\text{GeV}$, $\Gamma/M = 0.05$ and $R = 0.06$.

where $\mathcal{L}_{gg}(x) = \int_x^1 dy\,(x/y) f_{g/p}(y) f_{g/p}(x/y)$ is the gg parton luminosity and $\hat{\sigma}_{\text{cont,sig}}$ are the parton-level cross sections. We use CT10NNLO PDF set [96]. The signal cross-section $\hat{\sigma}_{\text{sig}}$, the deviation from the SM background, consists of the resonance-squared and the resonance-continuum interference [93],

$$\hat{\sigma}_{\text{sig}}(\hat{s}) = \frac{M^4}{(\hat{s}-M^2)^2 + M^2\Gamma^2}\left[\left(1 + \frac{2\Gamma}{RM} s_\phi\right)\hat{\sigma}_{\text{res}} + \frac{2(\hat{s}-M^2)c_\phi}{M^2}\hat{\sigma}_{\text{int}}\right], \tag{2.2}$$

where $s_\phi = \sin\phi$ and $c_\phi = \cos\phi$, and we factor out Breit-Wigner (BW) parts. We define $\hat{\sigma}_{\text{res,int}}$ and the relative phase ϕ in terms of phase-space integrated squared amplitudes ($\mathcal{M}_i = \mathcal{A}_i e^{i\phi_i}$)

$$\hat{\sigma}_{\text{int}} e^{i\phi} \equiv \frac{1}{32\pi\hat{s}} \int d\cos\theta^* \sum \mathcal{A}_{\text{cont}} \mathcal{A}_{\text{res}} e^{i(\phi_{\text{res}} - \phi_{\text{cont}})}, \tag{2.3}$$

$$\hat{\sigma}_{\text{res}} \equiv \frac{1}{32\pi\hat{s}} \int d\cos\theta^* \sum \mathcal{A}_{\text{res}}^2, \tag{2.4}$$

where θ^* is the scattering angle in the c.m. frame, and the summation is over helicity and color indices. We introduce a ratio R, defined by

$$R \equiv \frac{\hat{\sigma}_{\text{res}}}{\hat{\sigma}_{\text{int}}} \approx \frac{\mathcal{A}_{\text{res}}}{\mathcal{A}_{\text{cont}}}, \tag{2.5}$$

which measures the relative size of interference.

The shape of the invariant mass distribution is determined by the relative phase ϕ. In figure 2, we present the $m_{\gamma\gamma}$ distribution for various ϕ's with $M = 750\,\text{GeV}$, $\Gamma/M = 0.05$ and $R = 0.06$ at the 13 TeV LHC. The left panel corresponds to the cases for purely real ϕ or purely imaginary ϕ. We find that $\phi = 0$ ($\phi = 180°$) yields a dip-peak (peak-dip) structure. If $\phi = 90°$, an enhanced peak structure appears. $\phi = 270°$ generates a reduced

JHEP05(2016)009

BW-type peak (when $2\Gamma < RM$) or a dip (when $2\Gamma > RM$). In the right panel, more general cases with both real-part and imaginary-part interferences are considered. The $\phi = 45^\circ$ ($\phi = 135^\circ$) case, which can be considered as the deviated one from $\phi = 90^\circ$ toward $\phi = 0$ ($\phi = 180^\circ$), yields a shifted peak into higher (lower) mass, accompanying a mild dip. On the other hand, the $\phi = 315^\circ$ ($\phi = 225^\circ$) case shifts the dip into lower (higher) mass, with a mild peak.

Finite bin sizes in real experiments, however, limit the measurement of the full $m_{\gamma\gamma}$ distribution. The crucial factor is the total width of the resonance particle. For a narrow resonance, the real part interference, the term proportional to c_ϕ in eq. (2.2), is washed out after the integration over $m_{\gamma\gamma}$. Since the invariant mass distribution is highly accumulated near the resonance peak, we can consider parameters R, ϕ and parton luminosity as constant values. Then the total signal rate with the interference effect, defined as $\sigma_{\rm mNWA}$, is obtained as [93]

$$\sigma_{\rm mNWA} = \sigma_{\rm NWA} \cdot C = \left[\frac{M\pi}{\Gamma}\mathcal{L}_{gg}(M^2/s)\hat{\sigma}_{\rm res}(M^2)\right] \cdot C, \quad \text{for a narrow resonance,} \tag{2.6}$$

where $C = (1 + \frac{2\Gamma}{RM}s_\phi)$ quantifies the strength of the imaginary-part interference. Note that the terms inside the square bracket corresponds to the usual total rate in the narrow width approximation (NWA), production cross section times branching ratio. The subscript mNWA represents *modified* NWA. It is useful to express $\hat{\sigma}_{\rm sig}(\hat{s})$ in terms of $\sigma_{\rm mNWA}$ which is measured in experiments:

$$\hat{\sigma}_{\rm sig}(\hat{s}) = \frac{\Gamma M^3/(\pi\mathcal{L}_{gg}(M^2/s))}{(\hat{s}-M^2)^2 + M^2\Gamma^2}\left[\frac{2(\hat{s}-M^2)}{M^2}\frac{c_\phi}{RC} + 1\right] \cdot \sigma_{\rm mNWA}\,. \tag{2.7}$$

This is our resonance shape function for a narrow resonance.

For a broad resonance, with $\Gamma \gtrsim 50\,\text{GeV}$, we now need to take into account the $m_{\gamma\gamma}$ dependence of R, ϕ and parton luminosity; they are not constant in $m_{\gamma\gamma}$ anymore. We redefine the total rate $\sigma_{\rm mNWA}$ for a broad resonance by the integrated differential rate around the resonance mass M:

$$\sigma_{\rm mNWA} = \int_{M-\Delta}^{M+\Delta} dm_{\gamma\gamma}\left[\frac{d\sigma_{\rm sig}}{dm_{\gamma\gamma}}\right], \quad \text{for a broad resonance,} \tag{2.8}$$

where $\sigma_{\rm sig}$ is given in eq. (2.1). We set $\Delta = 100\,\text{GeV}$ for our broad resonance example. We also use the following ratio

$$K_{\rm intf} = \frac{\sigma_{\rm mNWA}}{\sigma_{\rm prod}\cdot \text{Br}_{\gamma\gamma}} \tag{2.9}$$

to quantify the strength of the imaginary-part interference for a broad resonance. This $K_{\rm intf}$ factor is approximately equal to the C factor for a narrow resonance in eq. (2.6).

The resonance shape function is parameterized not only by usual mass M, width Γ and the total rate $\sigma_{\rm mNWA}$ but also by the relative interference phase ϕ. R is not a completely independent parameter as shall be discussed. The purely real-part (imaginary-part) interference corresponds to $\phi = 0, 180^\circ$ ($\phi = \pm 90^\circ$). The real-part interference induces peak-dip or dip-peak structure in addition to a BW peak while the imaginary-part interference either enhances or reduces the BW peak or convert the peak to a BW

JHEP05(2016)009

dip [93]. Thus, the purely real-part interference can most significantly change the resonance shape from a BW peak while the purely imaginary-part interference can most significantly enhance the signal rate (or peak height). These two effects are our main topics. We will study two benchmark models for each of them.

It is hard to carry out a model-independent best-fit analysis including interference effects based on eq. (2.2) and eq. (2.7). The interference depends not only on M, Γ, $\sigma_{\rm mNWA}$, which are usually chosen in model-independent analysis without interference effects, but also on ϕ and R. In particular, R is correlated with $\sigma_{\rm mNWA}$, which is hard to obtain the analytic relation. In this regard we use two benchmark models to numerically discuss the interference effects. For the (purely) real-part interference, we consider a singlet model which introduces a CP-odd SM singlet scalar with a minimal set of vector-like quarks and vector-like leptons: see section 3. For the (purely) imaginary-part interference, Type II 2HDM with vector-like leptons is to be studied: section 4.

We also comment on our implementation of higher-order corrections. We first compare our LO total rate without interferences to the result obtained by `HIGLU` fortran package [97], which includes next-to-next-to-leading-order QCD and next-to-leading-order EW contributions, to obtain the correction factor. Then we multiply the same correction factor to the resonance-square term $\hat{\sigma}_{\rm res}$ and the interference term $\hat{\sigma}_{\rm int}$. Although this assumption approximately accounts for higher-order corrections to the total rate, it implies that $R = \hat{\sigma}_{\rm res}/\hat{\sigma}_{\rm int}$ does not receive appreciable higher-order corrections. It is reasonable to expect a substantial cancelation of higher order correction between $\hat{\sigma}_{\rm res}$ and $\hat{\sigma}_{\rm int}$. We relegate any existing correction of R to the theoretical uncertainty due to lacking of higher order calculation for interference term. In any case, both the real-part and the imaginary-part interferences approximately grow with $1/R$. Thus, any corrections to R would directly affect what we discuss in this paper.

2.2 Dataset and method

In order to quantitatively study interference effects on the 750 GeV diphoton excess data, we perform a Poissonian likelihood analysis to find the best fit. The dataset is from the latest LHC 8 and 13 TeV diphoton resonance search at around $m_{\gamma\gamma} = 750\,\text{GeV}$ of both ATLAS and CMS experiments. We read in the predicted backgrounds and observed data from the reported plots in refs. [1, 2, 98, 99]. The total uncertainty in each bin is assumed to be 2 (1.5) $\times$ statistical uncertainty for LHC 13 (8) TeV data.

The fit ranges considered in this paper are

$$\begin{aligned} m_{\gamma\gamma} &= \{630,\, 830\}\,\text{GeV} \quad \text{for ATLAS 13 (3.2/fb), CMS 13 (2.6/fb), CMS 8 (19.7/fb),} \\ m_{\gamma\gamma} &= \{642,\, 835\}\,\text{GeV} \quad \text{for ATLAS 8 (20.3/fb).} \end{aligned} \tag{2.10}$$

We choose ATLAS 8 data bins closest to 630 and 830 GeV. The range is somewhat broad so that we can consider a broad resonance as well. CMS 13 dataset is divided into CMS EBEB 13 and CMS EBEE 13 categories depending on which parts of detectors identify photons. We consider them as independent datasets. Fiducial signal efficiencies are taken from the experimental references and ref. [3].

JHEP05(2016)009

We carry out a χ^2-fit to all the data bins within the range, and take the total change of χ^2 compared to the SM-fit (background-only), $\Delta\chi^2 = \chi^2 - \chi^2_{\rm SM}$, as a measure of how well the model fits the data. Our SM-fit (background-only) results are:

$$\chi^2_{\rm SM} = 7.02,\ 4.93,\ 17.77,\ 1.52,\ 16.65, \tag{2.11}$$

for ATLAS 13, CMS EBEB 13, CMS EBEE 13, ATLAS 8, and CMS 8, respectively. The results are, of course, sensitive to the assumption of total uncertainties. ATLAS 13 and CMS EBEB 13 data are fitted better with a new resonance at around 750 GeV, but CMS EBEE 13 and CMS 8 data do not strongly support a new resonance — various excesses and deficits around 750 GeV do not significantly prefer a new resonance. Our read-in data and model-independent fit results without interferences approximately agree with those in ref. [3].

3 Singlet Model: real-part interference

3.1 Singlet Model

Consider a CP-odd SM-singlet scalar $\Phi = A$ which couples to vector-like quarks $Q \equiv Q^{7/6} = (\mathbf{3}, \mathbf{2}, 7/6)$ and vector-like leptons $L \equiv L^{3/2} = (\mathbf{1}, \mathbf{2}, 3/2)$:

$$-\mathcal{L} \ni \frac{1}{2}M_\Phi^2\Phi^2 + \sum_Q (s_Q\Phi + M_Q)\overline{Q}\gamma_5 Q + \sum_L (s_L\Phi + M_L)\overline{L}\gamma_5 L, \tag{3.1}$$

where $s_{Q,L}$ are real Yukawa couplings, $M_{\Phi,Q,L}$ mass eigenvalues, $N_{Q,L}$ number of fermions, and $q_{Q,L}$ electric charges. We choose $Q^{7/6}$ and $L^{3/2}$ from the minimal matter list [100] — the list of new particles that can eventually decay to SM particles — since they have the largest electric charges. We consider A, but H shall also exhibit similar effects.

In the quark sector, we introduce a single vector-like Q with fixed parameters

$$M_Q = 1\,\text{TeV},\ N_Q = 2,\ s_Q = 0.2. \tag{3.2}$$

We still have enough lepton sector free parameters that we can use to fit the data and to illustrate interference effects.

In the lepton sector, we consider

$$M_L = 400\,\text{GeV},\ N_L = 6,\ s_L \text{ is varied}. \tag{3.3}$$

The sign of the Yukawa s_L determines the sign of the relative phase: $s_L \to -s_L$ approximately changes the relative phase $\phi \to \pi + \phi$. It is an approximate relation because Q also contributes to the $\Phi \to \gamma\gamma$ part although it is subdominant to the L contribution. We will compare the results with positive and negative s_L (as well as with the results without any interference accounted for) to see how the best-fit changes with interference effects. Although we only need $N \geq 2$ to make $\text{BR}(\Phi \to \gamma\gamma) \gtrsim 90\%$, we also want to make Φ broad enough by having large enough N, as will be discussed below.

JHEP05(2016)009

Another important parameter is the width. In the above model, the width is typically too small ($\lesssim 1\,\text{GeV}$) to make interference effects apparent in current experiments; Φ mainly decays to loop-induced gg and $\gamma\gamma$

$$\Gamma(\Phi \to gg) = \frac{\alpha_S^2}{128\pi^3}\frac{M_\Phi^3}{M_Q^2}\left|\sum_Q s_Q A_{1/2}^\Phi\left(\frac{M_\Phi^2}{4M_Q^2}\right)\right|^2, \tag{3.4}$$

$$\Gamma(\Phi \to \gamma\gamma) = \frac{\alpha^2}{256\pi^3}M_\Phi^3\left|\sum_{f=Q,L} N_C\, q_f^2\frac{s_f}{M_f}A_{1/2}^\Phi\left(\frac{M_\Phi^2}{4M_f^2}\right)\right|^2, \tag{3.5}$$

where loop functions $A_{1/2}^{\Phi=A}$ are defined as in ref. [101], and other signals such as $Z\gamma$, ZZ, WW are currently well below their LHC 8 sensitivities. If such a narrow resonance falls within a single experimental bin, the real-part interference (although itself is independent on the width) is cancelled out. In addition, the imaginary-part interference is small since it is directly proportional to the width as $(C-1) \propto \Gamma$. Thus, to illustrate the impacts of interference effects, we assume a bigger constant width

$$\Gamma_\Phi = 5\,\text{GeV}, \tag{3.6}$$

which is easily accomplished by adding extra hidden decay modes of Φ, not constrained at all [102]. We cannot assume an arbitrarily large new decay width because diphoton signal will then be relatively suppressed. If the N_L is smaller, the total width decreases and the interference effects will be less significant. Meanwhile, for $M_L \leq M_\Phi/2$, the decays into vector-like leptons dominate and the diphoton signal becomes too suppressed. Although such light leptons can change the phase ϕ and introduce different interference effects, we cannot fit the diphoton excess data well and do not discuss this possibility further.

An important feature of the singlet scalar model is

$$\phi \simeq \begin{cases} 8.3^\circ & \text{for } s_L > 0; \\ 188.3^\circ & \text{for } s_L < 0, \end{cases} \tag{3.7}$$

which induces almost purely real-part interference. This is the case in which resonance shape is maximally distorted from pure BW shape (and the peak location is maximally shifted), for the given total rate. The small but non-zero phase is generated from the SM quark loops in $gg \to \gamma\gamma$ background box diagrams.

3.2 Results — Singlet Model

In figure 3 we show an example of the SM-singlet scalar resonance shapes for $s_L > 0$ (blue-solid) and $s_L < 0$ (red-dashed) with full interference effects. For comparison, we also show the resonance shape without interference (green-dotted). All three cases have the same NWA rates and the width Γ_Φ. But $s_L > 0$ ($s_L < 0$) induces a small dip-peak (peak-dip) interference pattern added to the BW peak, so that a long tail toward a high (low) invariant mass region appears and the peak shifts toward the same direction. As a result, the best-fit results change, even with the same NWA rates, masses and widths. We

JHEP05(2016)009

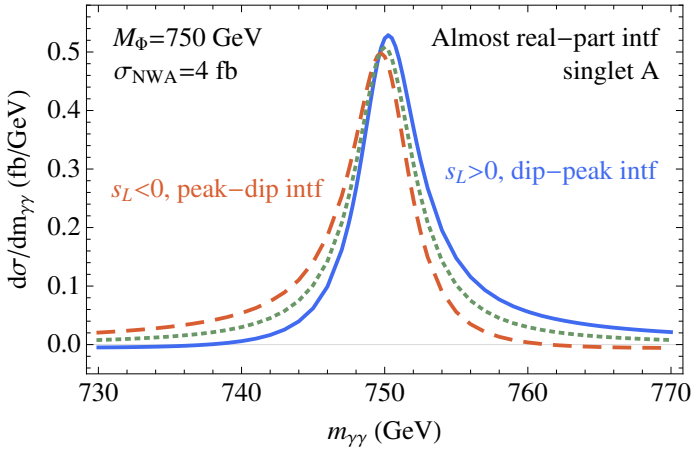

Figure 3. Example diphoton resonance shapes with $s_L > 0$ (dip-peak interference, *blue-solid*), $s_L < 0$ (peak-dip interference, *red-dashed*), and no interference (*green-dotted*) for the same mass $M_\Phi = 750\,\text{GeV}$ and the NWA rate $\sigma_{\rm NWA} \simeq 4\,\text{fb}$. The relative phase $\phi \simeq 8.3°(188.3°)$ for $s_L > 0(< 0)$ induces almost purely real-part interference, and the resulting peak shifts and long tails affect best-fit analysis. The small imaginary-part interference also makes true observable mNWA rates $\sigma_{\rm mNWA}$ and peak heights slightly different. We set $|s_L| \simeq 1.5$ and $\Gamma_\Phi = 5\,\text{GeV}$.

quantify such interference effects in this subsection. The small but non-zero imaginary-part interference, eq. (3.7), actually makes $\sigma_{\rm mNWA}$ (true observable rate defined in eq. (2.6)) and the peak heights slightly different among the three shapes.

Figure 4 shows the 68% and 95% CL allowed regions from individual ATLAS 13 (left) and CMS EBEB 13 (right) datasets, for a singlet scalar $\Phi = A$ model with $s_L > 0$ (upper) and $s_L < 0$ (lower). For comparison, we also show the results without any interferences accounted for (dashed). These datasets are the ones that most strongly prefer the existence of a 750 GeV resonance. And the interference effect does not change the preference of a new resonance contribution; the data fit still better with a new resonance even with interference effects. Comparing the upper panels for $s_L > 0$ with the lower panels for $s_L < 0$, we find that the 68% CL best-fit mass parameter is shifted by about 1–4 GeV while a much bigger shift $\mathcal{O}(1)$ GeV is expected for the 95% CL region. The shift is also bigger for weaker couplings s_L because the signal is smaller and R is relatively bigger. For $s_L > 0$ producing a dip-peak interference, the resonance peak location shifts toward a higher mass region (see figure 3); consequently, a somewhat smaller mass parameter can fit the data most well. Meanwhile, the best-fit coupling strength is not significantly changed with both signs of interference effects.

In figure 5, we investigate the interference effects in the whole dataset including LHC 13 and LHC 8 dataset that do not strongly prefer the existence of a new resonance. The 68% C.L. allowed regions again shift due to the interference by about 1–4 GeV and a bigger shift is expected for the 95% CL region or for weaker couplings s_L. The preference of an additional resonance still exists.

There is a noticeable tendency that interference effects become stronger with a weaker s_L, as can be deduced from a wider best-fit mass shift with smaller s_L in figure 4 and

JHEP05(2016)009

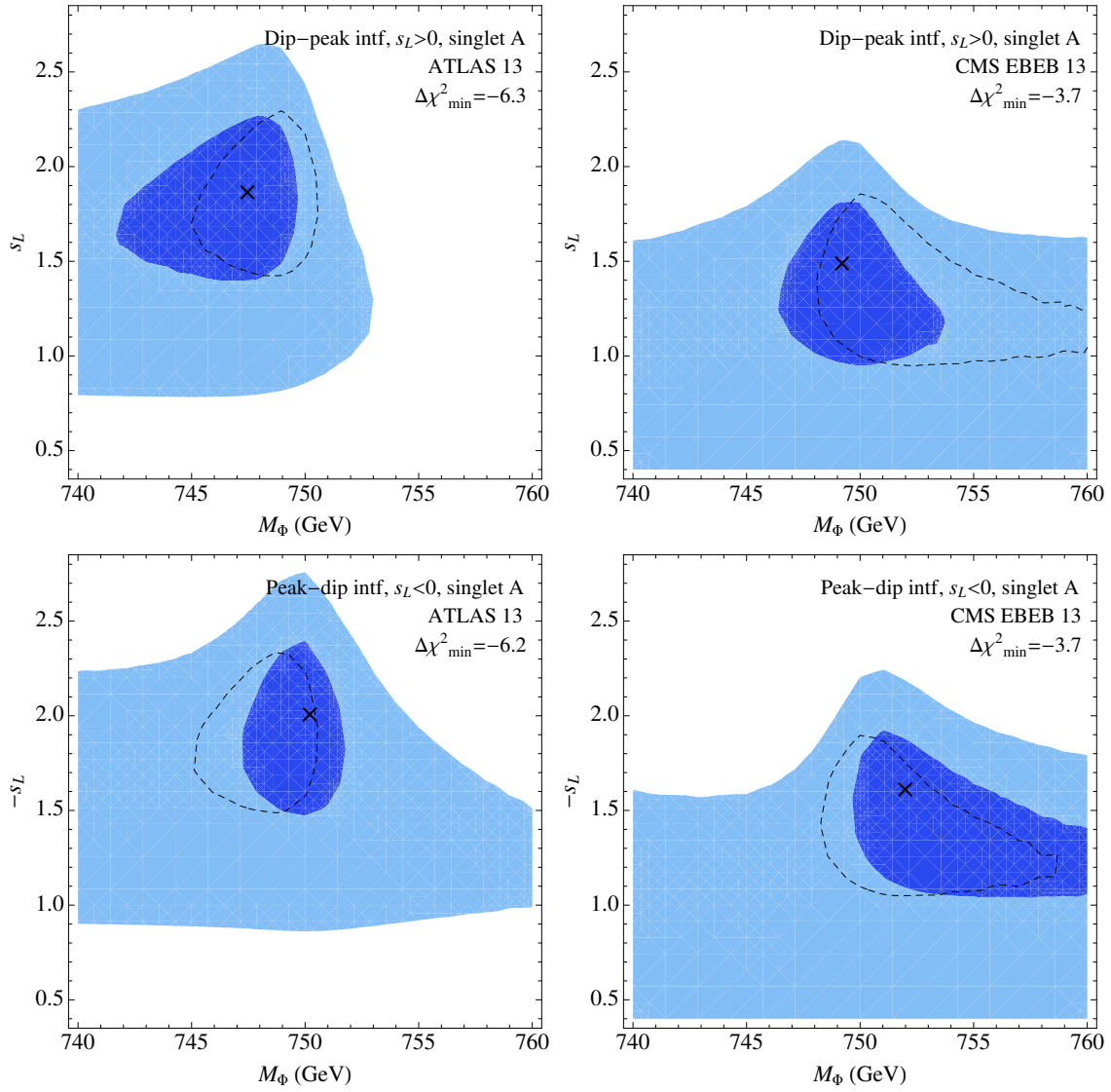

Figure 4. The 68% CL(darker blue) and 95% CL(lighter blue) preferred regions for CP-odd singlet A. $s_L > 0$ (*upper*) and $s_L < 0$ (*lower*) can be compared with each other (and with dashed lines for the 68% CL results without interferences accounted for) to see interference strength. Γ_Φ=5 GeV. Fit is performed for $m_{\gamma\gamma} = 630 - 830\,\text{GeV}$ from ATLAS 13 (*left*, $\chi^2_{\rm SM} = 7.02$) and CMS EBEB 13 (*right*, $\chi^2_{\rm SM} = 4.93$) datasets. The best-fit mass ranges with positive and negative s_L differ by $\mathcal{O}(1)\,\text{GeV}$ and the difference is bigger with weaker s_L. The best-fit $\Delta\chi^2_{\rm min}$ compared to the SM fit $\chi^2_{\rm SM}$ is also shown.

figure 5. This is a general result of interference; the real-part interference approximately grows with $1/R \sim \mathcal{A}_{\rm cont}/\mathcal{A}_{\rm res}$ amplitude ratio, which measures the background-resonance interference contribution compared to the resonance-squared contribution. If future data prefer a weaker signal, the interference effects will be larger and more important.

Finally, we briefly compare various best-fit results. Compared to the ATLAS 13 result in figure 4, the CMS EBEB 13 prefers a resonance with a slightly higher mass and weaker

JHEP05(2016)009

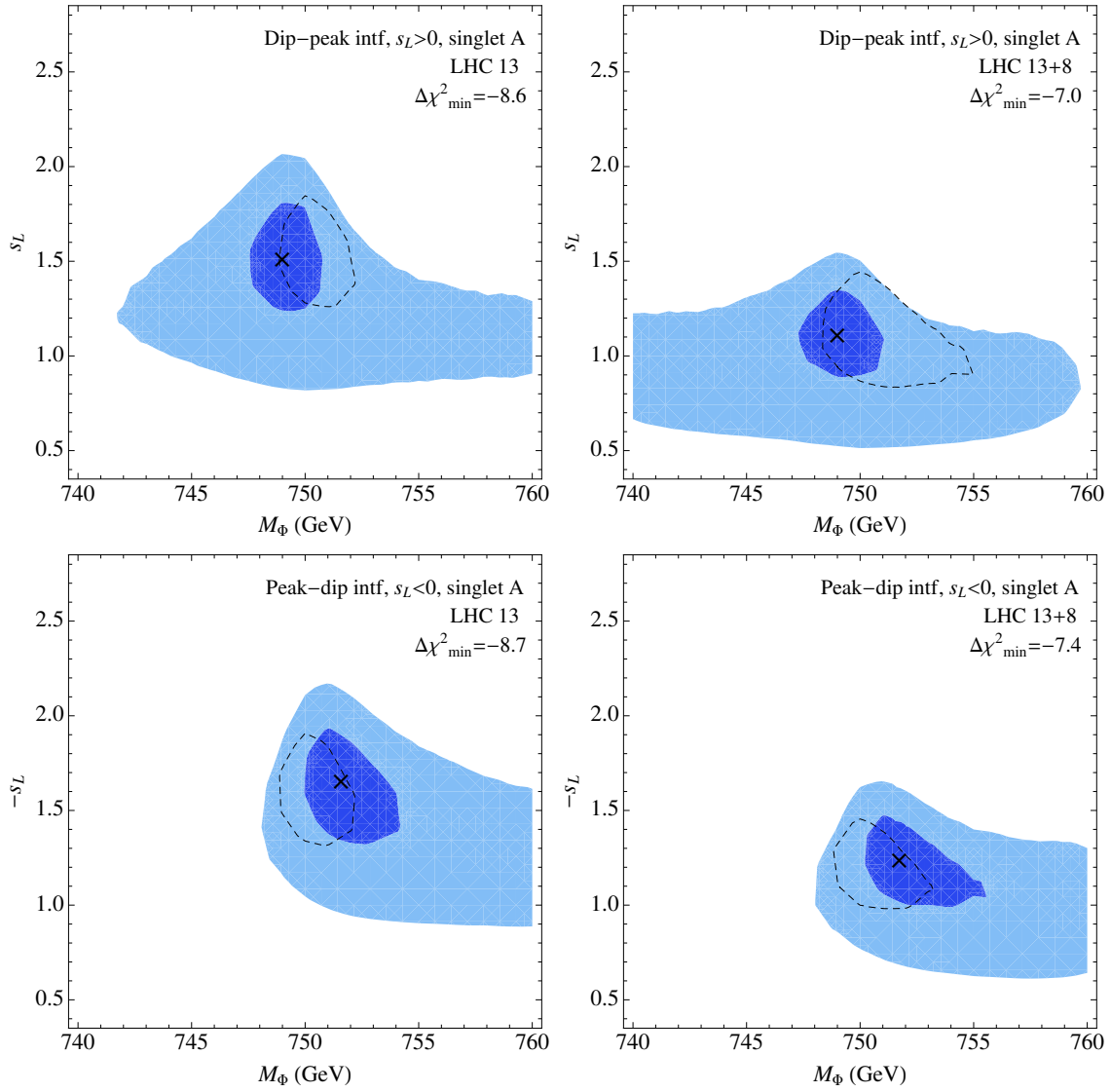

Figure 5. The 68% CL(darker blue) and 95% CL(lighter blue) preferred regions for CP-odd singlet A. $s_L > 0$ (*upper*) and $s_L < 0$ (*lower*) can be compared with each other (and with dashed lines for the 68% CL results without interferences accounted for) to see interference strength. Γ_Φ=5 GeV. Fit is performed for $m_{\gamma\gamma}$ = 630–830 GeV from LHC 13 (*left*, $\chi^2_{\rm SM}$ = 29.7) and LHC 13+8 (*right*, $\chi^2_{\rm SM}$ = 47.9) datasets. The best-fit mass ranges with positive and negative s_L differ by $\mathcal{O}(1)$ GeV and the difference is bigger with weaker s_L. The best-fit $\Delta\chi^2_{\rm min}$ compared to the SM fit $\chi^2_{\rm SM}$ is also shown.

coupling. But the preferences of a new resonance around 750 GeV from both data are consistent with each other. Including LHC 8 datasets in figure 5 significantly prefers a weaker coupling and actually worsens the best-fit (total $|\Delta\chi^2_{\rm min}|$ in the right panel decreased from the left panel). This may imply that the LHC 8 datasets do not strongly favor the resonance contribution.

JHEP05(2016)009

		$\mathrm{SU}(3) \times \mathrm{SU}(2) \times \mathrm{U}(1)_Y$
$L_L = \begin{pmatrix} E_L \\ D_L \end{pmatrix}$	$L_R = \begin{pmatrix} E'_R \\ D'_R \end{pmatrix}$	$(\mathbf{1}, \mathbf{2}, -\frac{3}{2})$
E_R	E'_L	$(\mathbf{1}, \mathbf{1}, -1)$
D_R	D'_L	$(\mathbf{1}, \mathbf{1}, -2)$

Table 1. The contents and quantum numbers of vector-like leptons in the VLL-2HDM model. The electric charges of the doublet components are $(-1, -2)$.

4 VLL-2HDM: imaginary-part interference

4.1 VLL-2HDM model

We consider the Type II two-Higgs-Double-Model (2HDM) [103, 104] in the alignment limit extended with extra vector-like leptons (VLL). We first summarize the Higgs sector and then introduce the VLL sector. The Higgs sector consists of three neutral Higgs bosons, h, H (scalar), A (pseudo-scalar) and two charged Higgs bosons $H^\pm$. Assuming h as the observed Higgs boson with mass 125 GeV, we focus the heavier Higgs bosons, H and A in this paper. To be consistent with electroweak precision data and to explain the 750 GeV diphoton excess, we consider a degenerate heavy Higgs bosons

$$M_\phi = M_H = M_A = 750\,\mathrm{GeV}. \tag{4.1}$$

Note that the top quark Yukawa couplings of H^0 and A^0 are inversely proportional to t_β in the alignment limit.

The observed diphoton excess rate of $\mathcal{O}(1)$ fb is too large to be explained in the original 2HDM with the perturbativity of Yukawa coupling [4, 86]. The alignment limit is efficient to enhance $\mathrm{Br}(H^0 \to \gamma\gamma)$ by forbidding $H^0 \to WW, ZZ$ decays. If t_β is small like ~ 1, the heavy Higgs bosons dominantly decay to the top pair, and the diphoton branching ratio is still very small such as $\mathrm{Br}(\phi \to \gamma\gamma) = 7.8\,(8.7) \times 10^{-6}$ for $\phi = H(A)$. The diphoton signal rate is just $\sigma(pp \to H/A \to \gamma\gamma) \simeq 0.01$ fb. If t_β is large, we may enhance the diphoton branching ratio by reducing $\mathrm{Br}(H/A \to t\bar{t})$, but the gluon fusion production cross section is also suppressed. In order to achieve the needed $\mathcal{O}(1)$ fb diphoton signal, we extend the model with extra VLLs, to be called the VLL-2HDM.

We now introduce VLLs, L_L, E_R, D_R, L_R, E'_L, D'_L, of which the quantum numbers are summarized in table 1. Note that the electric charges of $E^{(\prime)}$ and $D^{(\prime)}$ are -1 and -2, respectively. All of the VLLs in table 1 are imbedded in one family. In the following analysis we introduce 3 VLL families. The Lagrangian of the VLLs in Type II 2HDM is

$$\begin{aligned} -\mathcal{L} = {} & Y_D \overline{L}_L H_1 D_R + Y'_D \overline{L}_R H_1 D'_L + Y_E \overline{L}_L \tilde{H}_2 E_R + Y'_E \overline{L}_R \tilde{H}_2 E'_L \\ & + M_L \overline{L}_L L_R + M_E \overline{E}'_L E_R + M_D \overline{D}'_L D_R + \mathrm{h.c.} \end{aligned} \tag{4.2}$$

In this work we neglect the mixing between VLLs and the SM leptons although its phenomenological impact is interesting [105, 106].

JHEP05(2016)009

The mass matrix in the basis of (E, E') is

$$\mathcal{M}_E = \begin{pmatrix} M_L & \frac{1}{\sqrt{2}} Y_E v_2 \\ \frac{1}{\sqrt{2}} Y'_E v_2 & M_E \end{pmatrix} . \tag{4.3}$$

We have similar form of $\mathcal{M}_D$ by changing $Y_E^{(\prime)} \to Y_D^{(\prime)}, v_2 \to v_1, M_E \to M_D$. We consider the case where heavier mass eigenvalues are much larger than the lighter ones, for example, when $M_L \gg M_E, M_D$ or $Y_E^{(\prime)}, Y_D^{(\prime)} \gg 1$. Then, the contributions from the heavier mass eigenstates E_2 and D_2 are suppressed. For simplicity, we assume the two light mass eigenvalues are degenerated in mass, $(M_{E_1} = M_{D_1} = M)$. We do not consider the mass M below $M_\Phi/2$ since the new decay channels of $H/A \to E\bar{E}/D\bar{D}$ suppress the diphoton branching ratio quickly. We also assume that $Y_E = Y'_E$ and $Y_D = Y'_D$ for simplicity.

The Yukawa terms for the VLLs in the mass eigenstate basis become

$$\begin{aligned} -\mathcal{L}_{\text{Yukawa}} \supset & -\frac{1}{t_\beta} y_E H(\overline{E}_1 E_1 - \overline{E}_2 E_2) + t_\beta y_D H(\overline{D}_1 D_1 - \overline{D}_2 D_2) \\ & - i\frac{1}{t_\beta} y_E A(\overline{E}_1 \gamma_5 E_1 - \overline{E}_2 \gamma_5 E_2) - i\, t_\beta y_D A(\overline{D}_1 \gamma_5 D_1 - \overline{D}_2 \gamma_5 D_2) \\ & + y_E h(\overline{E}_1 E_1 - \overline{E}_2 E_2) + y_D h(\overline{D}_1 D_1 - \overline{D}_2 D_2) \,, \end{aligned} \tag{4.4}$$

where $y_E = -s_\beta s_{2\theta_E} Y_E/\sqrt{2}$, $y_D = -c_\beta s_{2\theta_D} Y_D/\sqrt{2}$, and the mixing angles $\theta_{E,D}$ are given by $\tan 2\theta_{E,D} = \sqrt{2} v_{2,1} Y_{E,D}/(M_L - M_{E,D})$.

The partial decay widths of $\Phi = h, H, A$ in the VLL-2HDM are

$$\Gamma(\Phi \to gg) = \frac{G_F \alpha_s^2 M_\Phi^3}{64\sqrt{2}\pi^3} \left| \sum_q \hat{y}_q^\Phi A_{1/2}^\Phi(\tau_q) \right|^2 , \tag{4.5}$$

$$\Gamma(\Phi \to \gamma\gamma) = \frac{G_F \alpha_e^2 M_\Phi^3}{128\sqrt{2}\pi^3} \left| \sum_q \hat{y}_q^\Phi N_c Q_q^2 A_{1/2}^\Phi(\tau_q) + \sum_\ell \hat{y}_\ell^\Phi Q_\ell^2 A_{1/2}^\Phi(\tau_\ell) + \mathcal{A}_{\gamma\gamma,\text{VLL}}^\Phi \right|^2 ,$$

where $\tau_f = M_\Phi^2/(4m_f^2)$, the relative Yukawa couplings normalized by the SM values are $\hat{y}_{t,b,\tau}^h = 1$, $\hat{y}_t^{H,A} = \mp 1/t_\beta$ and $\hat{y}_{b,\tau}^{H,A} = t_\beta$ for Type II in the aligned 2HDM, and the loop functions $A_{1,1/2}^{H/A}(\tau)$ are referred to ref. [101]. The VLL contributions $\mathcal{A}_{\gamma\gamma,\text{VLL}}^\Phi$ in eq. (4.5) are given as

$$\mathcal{A}_{\gamma\gamma,\text{VLL}}^\Phi = \sum_{\text{VLL}} \sum_{i=1,2} \left[Q_{E_i}^2 \frac{\hat{y}_t^\Phi y_E v}{M_{E_i}} A_{1/2}^\Phi(\tau_{E_i}) + Q_{D_i}^2 \frac{\hat{y}_b^\Phi y_D v}{M_{D_i}} A_{1/2}^\Phi(\tau_{D_i}) \right] . \tag{4.6}$$

We vary M from 375 GeV to 600 GeV and $y_{E,D}$ from -4π to 4π.

The final comment is on the constraint from the Higgs precision data. As shown eq. (4.5), the VLL loop also contributes to $h \to \gamma\gamma$, which is already very limited by the 8 TeV LHC data. If two Yukawa couplings y_D and y_E are tuned as

$$y_D = -\frac{Q_E^2}{Q_D^2} y_E = -0.25 y_E \,, \tag{4.7}$$

new contribution to the Higgs precision data vanishes. If $t_\beta = 1$, the cancellation of the VLL contributions to $h \to \gamma\gamma$ equally happens to the $A \to \gamma\gamma$ decay. Since the A diphoton signal is usually larger than the H signal if there is no cancellation, we choose $t_\beta = 0.7$ in the analysis. This small t_β and thus enhanced top quark Yukawa couplings of H and A shall bring about the excesses in the $t\bar{t}$ resonance searches. At the 8 TeV LHC, we find that the C factor for $gg \to H(A) \to t\bar{t}$ is -0.53 (-0.76), which yields about $\sigma \cdot \mathrm{Br} \simeq -430$ fb. This is under the LHC8 upper bound of 550 fb [107]. Other exclusion limits from $Z\gamma$ [108], $b\bar{b}$ [109], $\tau^+\tau^-$ [110], and jj [111] channels at the 8 TeV LHC are also satisfied in the parameter space under consideration.

4.2 Results — VLL-2HDM model

We first discuss the total widths of H and A, both of which are dominated by the $t\bar{t}$ decay channel. Using the running top quark mass $m_t(\mu = 750\,\mathrm{GeV}) = 147\,\mathrm{GeV}$ [112], we have $\Gamma_{H(A)} = 46(58)\,\mathrm{GeV}$. Since the degenerate H and A do not interfere, we regard them as independent resonances and superpose those resonance distributions. We perform a minimum χ^2 analysis (see section 2.2) and find the best-fit signal rates to the LHC 13+8 datasets

$$\sigma(pp \to \Phi \to \gamma\gamma) = \begin{cases} 6.5 \pm 2.5 \text{ fb } (68\%\text{CL}) \\ 6.5^{+4.5}_{-3.5} \text{ fb } (95\%\text{CL}) \end{cases}, \tag{4.8}$$

which are in agreement with ref. [3].

In our scenario of VLL-2HDM the relative interference phase is close to $\pm 90°$, corresponding to the imaginary interference. The interference between the H resonance and the continuum background, for example, yields $\phi \in [103°, 117°]$ for $y_E = 1$ and $\phi \in [-129°, -110°]$ for $y_E = -1$. The reasons are as follows. The complex phase from the continuum background amplitude is minor [94]. The production part $gg \to H/A$ generates large complex phase due to the top quark loop: $77°(91°)$ for $M_H(M_A) = 750\,\mathrm{GeV}$. The decay part $H(A) \to \gamma\gamma$ gives small phase $\sim 20°(30°)$ from the top quark loop, because the dominant contributions from VLL are *real*: note $M_{H,A} < 2M_L$. Depending on the sign of Yukawa coupling y_E, the whole complex phase is changed by π. It maximally enhances the signal rate for $\phi \approx 90°$ (constructive interference) and maximally suppress the signal rate for $\phi \approx -90°$ (destructive interference).

Figure 6 shows our results in the parameter space (y_E, M) for the VLL-2HDM. In the upper panels, the contours of the K_{intf} (green solid lines) defined in eq. (2.9) and the modified NWA rate (red dashed lines) are presented. Considering the observed *excess* of diphoton signal, σ_{mNWA} for K_{intf} is obtained only for the excess region over the continuum background. For comparison, the 68% C.L. allowed parameter space is also presented. It is of great interest that quite large interference effects, i.e., large $(K_{\mathrm{intf}} - 1)$, appear around the measured total signal rate, as shown in figures 6(a) and (b). For $y_E > 0$, $K_{\mathrm{intf}} > 1$ and thus constructive interference occurs: the interference enhances the signal by factor of 2 for the 3 fb total rate. Within the allowed region at 68% C.L., the interference effect ranges from 40% to 80% when $y_E > 0$. For $y_E < 0$, $K_{\mathrm{intf}} < 1$ so that destructive interference occurs: in order to explain the signal rate, we need quite large magnitude of y_E and thus very limited parameter space is allowed.

JHEP05(2016)009

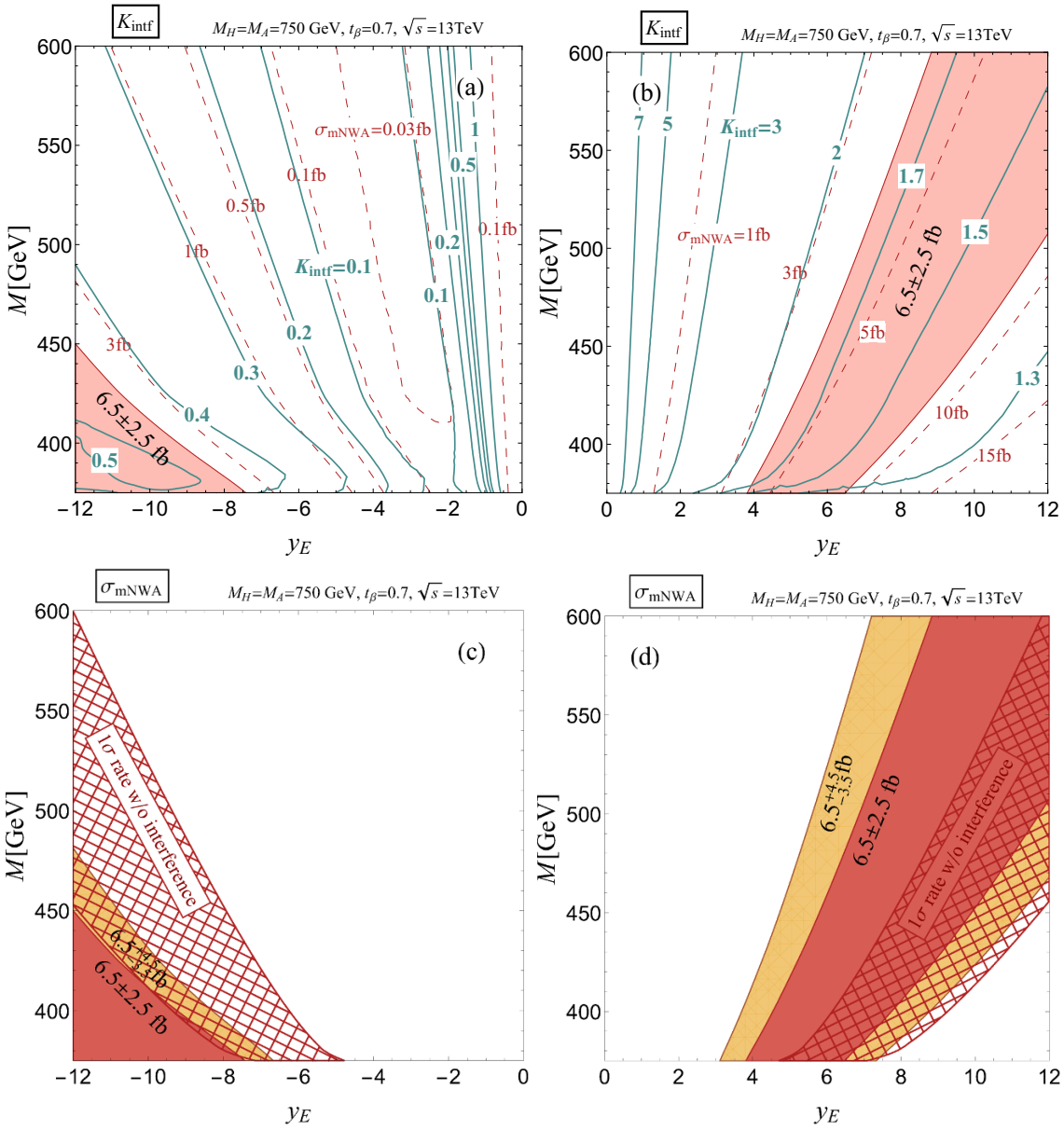

Figure 6. (*Upper*): contour plots for $K_{\rm intf}$ (solid lines) and $\sigma_{\rm mNWA}$ (dashed line) in the (y_E, M) plane of VLL-2HDM model. (*Lower*): the 68% CL(1σ, darker oranger) and 95% CL (lighter orange) best-fit regions are shown. For comparison, the 68% CL results without interferences accounted for are also shown as hatched regions. (*Left*): $y_E < 0$ induces signal suppression. (*Right*): $y_E > 0$ induces signal enhancement.

Figures 6(c) and (d) show the 1σ allowed region (red colored) and 2σ allowed region (yellow colored) with interference in the parameter space (y_E, M). In order to present the interference effect, the 1σ allowed region without interference (hatched) is also given. For both positive y_E and negative y_E cases, the interference affect the underlying physics quite significantly. With positive y_E and $M = 400\,\text{GeV}$, for example, y_E required for the signal rate 6.5 fb is reduced from ~ 7.5 to ~ 5.5 by including the interference effects. Equivalently, the required number of VLL family is also reduced from 4 to 3.

JHEP05(2016)009

M[GeV]	y_E	ϕ^H	ϕ^A	$K^H_{\rm intf}$	$K^A_{\rm intf}$	$K^{H+A}_{\rm intf}$	$\sigma^{H+A}_{\rm mNWA}$[fb]
457	2	99°	123°	2.6	5.9	3.5	1
413	4	93°	108°	1.6	3.0	2.0	3
400	6	91°	104°	1.3	2.1	1.6	6
385	−5	−96°	−88°	0.38	0.20	0.32	1
395	−8	−95°	−86°	0.54	0.21	0.43	3

Table 2. Numerical values for ϕ, $K_{\rm intf}$, and $\sigma_{\rm mNWA}$ for H, A and the total in the VLL-2HDM. The benchmark parameter points are chosen to yield total signal rates of $1, 3, 6$ fb.

In table 2, we present the numerical values for ϕ, $K_{\rm intf}$, and $\sigma_{\rm mNWA}$ for five benchmark parameter points. In order to see the individual interference effects, we show ϕ and $K_{\rm intf}$ separately for H and A. For both H and A, the relative interference phase is about $\pm 90°$: almost purely imaginary interference occurs. $K^H_{\rm intf}$ and $K^A_{\rm intf}$ show that the interference effects are larger for A than for H. This is because the A contribution is small due to the significant cancelations among VLL loops. The resulting small R (resonance to continuum ratio) yields large interference as can be seen in eq. (2.2). One crucial result is that the interference effects become larger with decreasing signal rate. For 1 fb signal rate, for example, the enhancement factor due to the interference can be as large as a factor of three. If the current signal rate is fluctuated up and the future precision measurements lead to lower signal rate, the interference effects become crucial.

Finally we make some comments on the interference effects in a higher order production process, the quark-gluon initiated one. Although the resonance signal rate S is smaller than that in the gluon fusion production, the tree-level continuum background $gq \to \gamma\gamma q$ has large rate B. The interference rate $\sim 2\sqrt{SB}$ can be non-negligible. Since this is a $2 \to 3$ process, our formalism based on the $m_{\gamma\gamma}$ distribution for a $2 \to 2$ process in eqs. (2.1) and (2.2) do not apply. Full analytic study of the interference effects in a $2 \to 3$ process is beyond the scope of this paper. Nevertheless estimating the interference signal rate in the gq process is required to validate our main results in figures 4, 5, and 6: if $\sigma^{\rm int}(qg \to \gamma\gamma j)$ is compatible with $\sigma^{\rm int}(gg \to \gamma\gamma)$, the preferred regions by the 750 GeV diphoton excess shall be changed. By using `MCFM` [113] for the SM continuum background rate B and the `HIGLU` for the pure resonance rate S, we perform a rough estimation for the interference effect, $2\sqrt{SB}$. Since the gq process is a reducible one, a hard jet with $p_T^j > 30$ GeV is vetoed. We find that $\sigma^{\rm int}(qg \to \gamma\gamma j)$ in the bin of $m_{\gamma\gamma} \in [700, 800]$ GeV is about 10% of the corresponding $\sigma^{\rm int}(gg \to \gamma\gamma)$. Our main results are not affected significantly.

5 Conclusions and discussions

We have investigated the impacts of the resonance-continuum interference in the $gg \to \gamma\gamma$ process on the recently observed 750 GeV diphoton excess. The two most important interference effects — signal enhancement from the purely imaginary-part interference and shape distortion from the purely real-part interference — have been studied in two benchmark models.

JHEP05(2016)009

First, a CP-odd singlet scalar with $\Gamma = 5\,\text{GeV}$ (extended with vector-like fermions) was considered to represent the purely real-part interference case. The model predicts that the 68%(95%) CL allowed mass range shifts by 1–4 (any $\mathcal{O}(1)$) GeV as a result of the interference. The shift is expected to be larger with a weaker coupling parameter space, which will be more preferred if the excess rate decreases in the future. Second, the heavy Higgs bosons in the two-Higgs-doublet-model with $\Gamma \sim 50\,\text{GeV}$ (extended with vector-like leptons) was considered to represent the purely imaginary-part interference case. In this case, the diphoton resonance signal is found to be enhanced or suppressed by a factor of 2(1.6) for 3(6) fb signal rate. Again, the effect is bigger for a weaker coupling parameter space.

Although our results are obtained with benchmark models, any scalar resonance in the $gg \to \gamma\gamma$ process with similar widths and total rates would exhibit similar sizes of interference effects. In addition, the relative phase ϕ between the resonance and the continuum will determine the type of interference effects. For the given diphoton rate and the phase ϕ, the total width is the most important parameter. If the width is much smaller than the current resolution $\sim \mathcal{O}(1)\,\text{GeV}$, the real-part interference will cancel out and the imaginary-part interference will be small in proportion to the width. If a resonance is very broad, a careful study of resonance shape including its $m_{\gamma\gamma}$-dependence should be carried out, based on our formalism and method presented in this paper.

The future precision shape measurements and interpretations taking into account the resonance-continuum interference can provide important information and consistency check of a new resonance. One cannot only test a BW resonance hypothesis but also measure ϕ and various other parameters that come into the interference effects. Remarkably, if any noticeable deviations from a BW shape can be fit well with the real-part interference, this would be another convincing evidence of a new resonance.

Acknowledgments

The work of SJ is supported by the US Department of Energy under contract DE-AC02-76SF00515. The work of JS is supported by NRF-2013R1A1A2061331. The work of YWY is supported by NRF-2012R1A2A1A01006053. We thank KIAS Center for Advanced Computation for providing computing resources.

References

[1] ATLAS collaboration, *Search for resonances decaying to photon pairs in 3.2 fb^{-1} of pp collisions at $\sqrt{s} = 13$ TeV with the ATLAS detector*, ATLAS-CONF-2015-081.

[2] CMS collaboration, *Search for new physics in high mass diphoton events in proton-proton collisions at $\sqrt{s} = 13$ TeV*, CMS-PAS-EXO-15-004.

[3] A. Falkowski, O. Slone and T. Volansky, *Phenomenology of a 750 GeV Singlet*, *JHEP* **02** (2016) 152 [arXiv:1512.05777] [INSPIRE].

JHEP05(2016)009

[4] S. Di Chiara, L. Marzola and M. Raidal, *First interpretation of the 750 GeV di-photon resonance at the LHC*, arXiv:1512.04939 [INSPIRE].

[5] K. Harigaya and Y. Nomura, *Composite Models for the 750 GeV Diphoton Excess*, *Phys. Lett.* **B 754** (2016) 151 [arXiv:1512.04850] [INSPIRE].

[6] A. Angelescu, A. Djouadi and G. Moreau, *Scenarii for interpretations of the LHC diphoton excess: two Higgs doublets and vector-like quarks and leptons*, *Phys. Lett.* **B 756** (2016) 126 [arXiv:1512.04921] [INSPIRE].

[7] Y. Nakai, R. Sato and K. Tobioka, *Footprints of New Strong Dynamics via Anomaly*, *Phys. Rev. Lett.* **116** (2016) 151802 [arXiv:1512.04924] [INSPIRE].

[8] S. Knapen, T. Melia, M. Papucci and K. Zurek, *Rays of light from the LHC*, *Phys. Rev.* **D 93** (2016) 075020 [arXiv:1512.04928] [INSPIRE].

[9] D. Buttazzo, A. Greljo and D. Marzocca, *Knocking on new physics' door with a scalar resonance*, *Eur. Phys. J.* **C 76** (2016) 116 [arXiv:1512.04929] [INSPIRE].

[10] A. Pilaftsis, *Diphoton Signatures from Heavy Axion Decays at the CERN Large Hadron Collider*, *Phys. Rev.* **D 93** (2016) 015017 [arXiv:1512.04931] [INSPIRE].

[11] R. Franceschini et al., *What is the $\gamma\gamma$ resonance at 750 GeV?*, *JHEP* **03** (2016) 144 [arXiv:1512.04933] [INSPIRE].

[12] J. Ellis, S.A.R. Ellis, J. Quevillon, V. Sanz and T. You, *On the Interpretation of a Possible $\sim$ 750 GeV Particle Decaying into $\gamma\gamma$*, *JHEP* **03** (2016) 176 [arXiv:1512.05327] [INSPIRE].

[13] B. Bellazzini, R. Franceschini, F. Sala and J. Serra, *Goldstones in Diphotons*, *JHEP* **04** (2016) 072 [arXiv:1512.05330] [INSPIRE].

[14] R.S. Gupta, S. Jäger, Y. Kats, G. Perez and E. Stamou, *Interpreting a 750 GeV Diphoton Resonance*, arXiv:1512.05332 [INSPIRE].

[15] T. Higaki, K.S. Jeong, N. Kitajima and F. Takahashi, *The QCD Axion from Aligned Axions and Diphoton Excess*, *Phys. Lett.* **B 755** (2016) 13 [arXiv:1512.05295] [INSPIRE].

[16] S.D. McDermott, P. Meade and H. Ramani, *Singlet Scalar Resonances and the Diphoton Excess*, *Phys. Lett.* **B 755** (2016) 353 [arXiv:1512.05326] [INSPIRE].

[17] M. Low, A. Tesi and L.-T. Wang, *A pseudoscalar decaying to photon pairs in the early LHC Run 2 data*, *JHEP* **03** (2016) 108 [arXiv:1512.05328] [INSPIRE].

[18] C. Petersson and R. Torre, *The 750 GeV diphoton excess from the goldstino superpartner*, *Phys. Rev. Lett.* **116** (2016) 151804 [arXiv:1512.05333] [INSPIRE].

[19] E. Molinaro, F. Sannino and N. Vignaroli, *Minimal Composite Dynamics versus Axion Origin of the Diphoton excess*, arXiv:1512.05334 [INSPIRE].

[20] B. Dutta, Y. Gao, T. Ghosh, I. Gogoladze and T. Li, *Interpretation of the diphoton excess at CMS and ATLAS*, *Phys. Rev.* **D 93** (2016) 055032 [arXiv:1512.05439] [INSPIRE].

[21] Q.-H. Cao, Y. Liu, K.-P. Xie, B. Yan and D.-M. Zhang, *A Boost Test of Anomalous Diphoton Resonance at the LHC*, arXiv:1512.05542 [INSPIRE].

[22] A. Kobakhidze, F. Wang, L. Wu, J.M. Yang and M. Zhang, *750 GeV diphoton resonance in a top and bottom seesaw model*, *Phys. Lett.* **B 757** (2016) 92 [arXiv:1512.05585] [INSPIRE].

[23] P. Cox, A.D. Medina, T.S. Ray and A. Spray, *Diphoton Excess at 750 GeV from a Radion in the Bulk-Higgs Scenario*, arXiv:1512.05618 [INSPIRE].

JHEP05(2016)009

[24] R. Martinez, F. Ochoa and C.F. Sierra, *Diphoton decay for a 750 GeV scalar boson in an U(1)′ model*, arXiv:1512.05617 [INSPIRE].

[25] D. Bečirević, E. Bertuzzo, O. Sumensari and R. Zukanovich Funchal, *Can the new resonance at LHC be a CP-Odd Higgs boson?*, *Phys. Lett.* **B 757** (2016) 261 [arXiv:1512.05623] [INSPIRE].

[26] J.M. No, V. Sanz and J. Setford, *See-Saw Composite Higgses at the LHC: Linking Naturalness to the 750 GeV Di-Photon Resonance*, arXiv:1512.05700 [INSPIRE].

[27] S.V. Demidov and D.S. Gorbunov, *On sgoldstino interpretation of the diphoton excess*, arXiv:1512.05723 [INSPIRE].

[28] W. Chao, R. Huo and J.-H. Yu, *The Minimal Scalar-Stealth Top Interpretation of the Diphoton Excess*, arXiv:1512.05738 [INSPIRE].

[29] S. Fichet, G. von Gersdorff and C. Royon, *Scattering Light by Light at 750 GeV at the LHC*, arXiv:1512.05751 [INSPIRE].

[30] D. Curtin and C.B. Verhaaren, *Quirky Explanations for the Diphoton Excess*, *Phys. Rev.* **D 93** (2016) 055011 [arXiv:1512.05753] [INSPIRE].

[31] L. Bian, N. Chen, D. Liu and J. Shu, *A hidden confining world on the 750 GeV diphoton excess*, arXiv:1512.05759 [INSPIRE].

[32] J. Chakrabortty, A. Choudhury, P. Ghosh, S. Mondal and T. Srivastava, *Di-photon resonance around 750 GeV: shedding light on the theory underneath*, arXiv:1512.05767 [INSPIRE].

[33] A. Ahmed, B.M. Dillon, B. Grzadkowski, J.F. Gunion and Y. Jiang, *Higgs-radion interpretation of 750 GeV di-photon excess at the LHC*, arXiv:1512.05771 [INSPIRE].

[34] C. Csáki, J. Hubisz and J. Terning, *Minimal model of a diphoton resonance: Production without gluon couplings*, *Phys. Rev.* **D 93** (2016) 035002 [arXiv:1512.05776] [INSPIRE].

[35] Y. Bai, J. Berger and R. Lu, *A 750 GeV Dark Pion: Cousin of a Dark G-parity-odd WIMP*, arXiv:1512.05779 [INSPIRE].

[36] R. Benbrik, C.-H. Chen and T. Nomura, *Higgs singlet boson as a diphoton resonance in a vectorlike quark model*, *Phys. Rev.* **D 93** (2016) 055034 [arXiv:1512.06028] [INSPIRE].

[37] J.S. Kim, J. Reuter, K. Rolbiecki and R. Ruiz de Austri, *A resonance without resonance: scrutinizing the diphoton excess at 750 GeV*, *Phys. Lett.* **B 755** (2016) 403 [arXiv:1512.06083] [INSPIRE].

[38] E. Gabrielli, K. Kannike, B. Mele, M. Raidal, C. Spethmann and H. Veermäe, *A SUSY Inspired Simplified Model for the 750 GeV Diphoton Excess*, *Phys. Lett.* **B 756** (2016) 36 [arXiv:1512.05961] [INSPIRE].

[39] A. Alves, A.G. Dias and K. Sinha, *The 750 GeV S-cion: Where else should we look for it?*, *Phys. Lett.* **B 757** (2016) 39 [arXiv:1512.06091] [INSPIRE].

[40] L.M. Carpenter, R. Colburn and J. Goodman, *Supersoft SUSY Models and the 750 GeV Diphoton Excess, Beyond Effective Operators*, arXiv:1512.06107 [INSPIRE].

[41] J. Bernon and C. Smith, *Could the width of the diphoton anomaly signal a three-body decay?*, *Phys. Lett.* **B 757** (2016) 148 [arXiv:1512.06113] [INSPIRE].

[42] W. Chao, *Symmetries Behind the 750 GeV Diphoton Excess*, arXiv:1512.06297 [INSPIRE].

JHEP05(2016)009

[43] M.T. Arun and P. Saha, *Gravitons in multiply warped scenarios — at 750 GeV and beyond*, arXiv:1512.06335 [INSPIRE].

[44] C. Han, H.M. Lee, M. Park and V. Sanz, *The diphoton resonance as a gravity mediator of dark matter*, *Phys. Lett.* **B 755** (2016) 371 [arXiv:1512.06376] [INSPIRE].

[45] M. Dhuria and G. Goswami, *Perturbativity, vacuum stability and inflation in the light of 750 GeV diphoton excess*, arXiv:1512.06782 [INSPIRE].

[46] H. Han, S. Wang and S. Zheng, *Scalar Explanation of Diphoton Excess at LHC*, *Nucl. Phys.* **B 907** (2016) 180 [arXiv:1512.06562] [INSPIRE].

[47] M.-x. Luo, K. Wang, T. Xu, L. Zhang and G. Zhu, *Squarkonium, diquarkonium and octetonium at the LHC and their diphoton decays*, *Phys. Rev.* **D 93** (2016) 055042 [arXiv:1512.06670] [INSPIRE].

[48] J. Chang, K. Cheung and C.-T. Lu, *Interpreting the 750 GeV diphoton resonance using photon jets in hidden-valley-like models*, *Phys. Rev.* **D 93** (2016) 075013 [arXiv:1512.06671] [INSPIRE].

[49] D. Bardhan, D. Bhatia, A. Chakraborty, U. Maitra, S. Raychaudhuri and T. Samui, *Radion Candidate for the LHC Diphoton Resonance*, arXiv:1512.06674 [INSPIRE].

[50] T.-F. Feng, X.-Q. Li, H.-B. Zhang and S.-M. Zhao, *The LHC 750 GeV diphoton excess in supersymmetry with gauged baryon and lepton numbers*, arXiv:1512.06696 [INSPIRE].

[51] W.S. Cho et al., *The 750 GeV Diphoton Excess May Not Imply a 750 GeV Resonance*, *Phys. Rev. Lett.* **116** (2016) 151805 [arXiv:1512.06824] [INSPIRE].

[52] D. Barducci, A. Goudelis, S. Kulkarni and D. Sengupta, *One jet to rule them all: monojet constraints and invisible decays of a 750 GeV diphoton resonance*, arXiv:1512.06842 [INSPIRE].

[53] I. Chakraborty and A. Kundu, *Diphoton excess at 750 GeV: Singlet scalars confront triviality*, *Phys. Rev.* **D 93** (2016) 055003 [arXiv:1512.06508] [INSPIRE].

[54] X.-F. Han and L. Wang, *Implication of the 750 GeV diphoton resonance on two-Higgs-doublet model and its extensions with Higgs field*, *Phys. Rev.* **D 93** (2016) 055027 [arXiv:1512.06587] [INSPIRE].

[55] O. Antipin, M. Mojaza and F. Sannino, *A natural Coleman-Weinberg theory explains the diphoton excess*, arXiv:1512.06708 [INSPIRE].

[56] F. Wang, L. Wu, J.M. Yang and M. Zhang, *750 GeV Diphoton Resonance, 125 GeV Higgs and Muon g-2 Anomaly in Deflected Anomaly Mediation SUSY Breaking Scenario*, arXiv:1512.06715 [INSPIRE].

[57] J. Cao, C. Han, L. Shang, W. Su, J.M. Yang and Y. Zhang, *Interpreting the 750 GeV diphoton excess by the singlet extension of the Manohar-Wise model*, *Phys. Lett.* **B 755** (2016) 456 [arXiv:1512.06728] [INSPIRE].

[58] F.P. Huang, C.S. Li, Z.L. Liu and Y. Wang, *750 GeV Diphoton Excess from Cascade Decay*, arXiv:1512.06732 [INSPIRE].

[59] J.J. Heckman, *750 GeV Diphotons from a D3-brane*, *Nucl. Phys.* **B 906** (2016) 231 [arXiv:1512.06773] [INSPIRE].

[60] X.-J. Bi, Q.-F. Xiang, P.-F. Yin and Z.-H. Yu, *The 750 GeV diphoton excess at the LHC and dark matter constraints*, arXiv:1512.06787 [INSPIRE].

JHEP05(2016)009

[61] J.S. Kim, K. Rolbiecki and R.R. de Austri, *Model-independent combination of diphoton constraints at 750 GeV*, arXiv:1512.06797 [INSPIRE].

[62] J.M. Cline and Z. Liu, *LHC diphotons from electroweakly pair-produced composite pseudoscalars*, arXiv:1512.06827 [INSPIRE].

[63] M. Bauer and M. Neubert, *Flavor Anomalies, the Diphoton Excess and a Dark Matter Candidate*, arXiv:1512.06828 [INSPIRE].

[64] M. Chala, M. Duerr, F. Kahlhoefer and K. Schmidt-Hoberg, *Tricking Landau-Yang: How to obtain the diphoton excess from a vector resonance*, *Phys. Lett.* **B 755** (2016) 145 [arXiv:1512.06833] [INSPIRE].

[65] S.M. Boucenna, S. Morisi and A. Vicente, *The LHC diphoton resonance from gauge symmetry*, arXiv:1512.06878 [INSPIRE].

[66] J. de Blas, J. Santiago and R. Vega-Morales, *New vector bosons and the diphoton excess*, arXiv:1512.07229 [INSPIRE].

[67] C.W. Murphy, *Vector Leptoquarks and the 750 GeV Diphoton Resonance at the LHC*, *Phys. Lett.* **B 757** (2016) 192 [arXiv:1512.06976] [INSPIRE].

[68] A.E.C. Hernández and I. Nisandzic, *LHC diphoton 750 GeV resonance as an indication of* $\mathrm{SU}(3)_c \times \mathrm{SU}(3)_L \times \mathrm{U}(1)_X$ *gauge symmetry*, arXiv:1512.07165 [INSPIRE].

[69] U.K. Dey, S. Mohanty and G. Tomar, *750 GeV resonance in the dark left-right model*, *Phys. Lett.* **B 756** (2016) 384 [arXiv:1512.07212] [INSPIRE].

[70] W.-C. Huang, Y.-L.S. Tsai and T.-C. Yuan, *Gauged Two Higgs Doublet Model confronts the LHC 750 GeV di-photon anomaly*, arXiv:1512.07268 [INSPIRE].

[71] S. Moretti and K. Yagyu, *750 GeV diphoton excess and its explanation in two-Higgs-doublet models with a real inert scalar multiplet*, *Phys. Rev.* **D 93** (2016) 055043 [arXiv:1512.07462] [INSPIRE].

[72] K.M. Patel and P. Sharma, *Interpreting 750 GeV diphoton excess in* SU(5) *grand unified theory*, *Phys. Lett.* **B 757** (2016) 282 [arXiv:1512.07468] [INSPIRE].

[73] S. Chakraborty, A. Chakraborty and S. Raychaudhuri, *Diphoton resonance at 750 GeV in the broken MRSSM*, arXiv:1512.07527 [INSPIRE].

[74] W. Altmannshofer, J. Galloway, S. Gori, A.L. Kagan, A. Martin and J. Zupan, *On the 750 GeV di-photon excess*, arXiv:1512.07616 [INSPIRE].

[75] M. Cvetič, J. Halverson and P. Langacker, *String Consistency, Heavy Exotics and the* 750 *GeV Diphoton Excess at the LHC*, arXiv:1512.07622 [INSPIRE].

[76] B.C. Allanach, P.S.B. Dev, S.A. Renner and K. Sakurai, *Di-photon Excess Explained by a Resonant Sneutrino in R-parity Violating Supersymmetry*, arXiv:1512.07645 [INSPIRE].

[77] K. Das and S.K. Rai, *The 750 GeV Diphoton excess in a* U(1) *hidden symmetry model*, arXiv:1512.07789 [INSPIRE].

[78] K. Cheung, P. Ko, J.S. Lee, J. Park and P.-Y. Tseng, *A Higgcision study on the 750 GeV Di-photon Resonance and 125 GeV SM Higgs boson with the Higgs-Singlet Mixing*, arXiv:1512.07853 [INSPIRE].

[79] J. Liu, X.-P. Wang and W. Xue, *LHC diphoton excess from colorful resonances*, arXiv:1512.07885 [INSPIRE].

JHEP05(2016)009

[80] L.J. Hall, K. Harigaya and Y. Nomura, *750 GeV Diphotons: Implications for Supersymmetric Unification*, *JHEP* **03** (2016) 017 [arXiv:1512.07904] [INSPIRE].

[81] A. Salvio and A. Mazumdar, *Higgs Stability and the 750 GeV Diphoton Excess*, *Phys. Lett.* **B 755** (2016) 469 [arXiv:1512.08184] [INSPIRE].

[82] C. Cai, Z.-H. Yu and H.-H. Zhang, *The 750 GeV diphoton resonance as a singlet scalar in an extra dimensional model*, arXiv:1512.08440 [INSPIRE].

[83] Q.-H. Cao, Y. Liu, K.-P. Xie, B. Yan and D.-M. Zhang, *The Diphoton Excess, Low Energy Theorem and the 331 Model*, arXiv:1512.08441 [INSPIRE].

[84] X.-J. Bi et al., *A Promising Interpretation of Diphoton Resonance at 750 GeV*, arXiv:1512.08497 [INSPIRE].

[85] P.S.B. Dev, R.N. Mohapatra and Y. Zhang, *Quark Seesaw, Vectorlike Fermions and Diphoton Excess*, *JHEP* **02** (2016) 186 [arXiv:1512.08507] [INSPIRE].

[86] S.K. Kang and J. Song, *Top-phobic heavy Higgs boson as the 750 GeV diphoton resonance*, arXiv:1512.08963 [INSPIRE].

[87] D.A. Dicus and S.S.D. Willenbrock, *Photon Pair Production and the Intermediate Mass Higgs Boson*, *Phys. Rev.* **D 37** (1988) 1801 [INSPIRE].

[88] L.J. Dixon and M.S. Siu, *Resonance continuum interference in the diphoton Higgs signal at the LHC*, *Phys. Rev. Lett.* **90** (2003) 252001 [hep-ph/0302233] [INSPIRE].

[89] S.P. Martin, *Shift in the LHC Higgs diphoton mass peak from interference with background*, *Phys. Rev.* **D 86** (2012) 073016 [arXiv:1208.1533] [INSPIRE].

[90] S.P. Martin, *Interference of Higgs diphoton signal and background in production with a jet at the LHC*, *Phys. Rev.* **D 88** (2013) 013004 [arXiv:1303.3342] [INSPIRE].

[91] L.J. Dixon and Y. Li, *Bounding the Higgs Boson Width Through Interferometry*, *Phys. Rev. Lett.* **111** (2013) 111802 [arXiv:1305.3854] [INSPIRE].

[92] F. Coradeschi et al., *Interference effects in the $H(\to \gamma\gamma) + 2$ jets channel at the LHC*, *Phys. Rev.* **D 92** (2015) 013004 [arXiv:1504.05215] [INSPIRE].

[93] S. Jung, J. Song and Y.W. Yoon, *Dip or nothingness of a Higgs resonance from the interference with a complex phase*, *Phys. Rev.* **D 92** (2015) 055009 [arXiv:1505.00291] [INSPIRE].

[94] S. Jung, Y.W. Yoon and J. Song, *Interference effect on a heavy Higgs resonance signal in the $\gamma\gamma$ and ZZ channels*, *Phys. Rev.* **D 93** (2016) 055035 [arXiv:1510.03450] [INSPIRE].

[95] ATLAS, CMS collaborations, *Combined Measurement of the Higgs Boson Mass in pp Collisions at $\sqrt{s} = 7$ and 8 TeV with the ATLAS and CMS Experiments*, *Phys. Rev. Lett.* **114** (2015) 191803 [arXiv:1503.07589] [INSPIRE].

[96] J. Gao et al., *CT10 next-to-next-to-leading order global analysis of QCD*, *Phys. Rev.* **D 89** (2014) 033009 [arXiv:1302.6246] [INSPIRE].

[97] M. Spira, *HIGLU: A program for the calculation of the total Higgs production cross-section at hadron colliders via gluon fusion including QCD corrections*, hep-ph/9510347 [INSPIRE].

[98] ATLAS collaboration, *Search for high-mass diphoton resonances in pp collisions at $\sqrt{s} = 8$ TeV with the ATLAS detector*, *Phys. Rev.* **D 92** (2015) 032004 [arXiv:1504.05511] [INSPIRE].

JHEP05(2016)009

[99] CMS collaboration, *Search for diphoton resonances in the mass range from 150 to 850 GeV in pp collisions at $\sqrt{s} = 8$ TeV*, *Phys. Lett.* **B 750** (2015) 494 [arXiv:1506.02301] [INSPIRE].

[100] E. Del Nobile, R. Franceschini, D. Pappadopulo and A. Strumia, *Minimal Matter at the Large Hadron Collider*, *Nucl. Phys.* **B 826** (2010) 217 [arXiv:0908.1567] [INSPIRE].

[101] A. Djouadi, *The anatomy of electro-weak symmetry breaking. I: The Higgs boson in the standard model*, *Phys. Rept.* **457** (2008) 1 [hep-ph/0503172] [INSPIRE].

[102] ATLAS collaboration, *Search for new phenomena in final states with an energetic jet and large missing transverse momentum in pp collisions at $\sqrt{s} = 8$ TeV with the ATLAS detector*, *Eur. Phys. J.* **C 75** (2015) 299 [*Erratum ibid.* **C 75** (2015) 408] [arXiv:1502.01518] [INSPIRE].

[103] J.F. Gunion and H.E. Haber, *The CP conserving two Higgs doublet model: The approach to the decoupling limit*, *Phys. Rev.* **D 67** (2003) 075019 [hep-ph/0207010] [INSPIRE].

[104] G.C. Branco, P.M. Ferreira, L. Lavoura, M.N. Rebelo, M. Sher and J.P. Silva, *Theory and phenomenology of two-Higgs-doublet models*, *Phys. Rept.* **516** (2012) 1 [arXiv:1106.0034] [INSPIRE].

[105] R. Dermisek, E. Lunghi and S. Shin, *Two Higgs doublet model with vectorlike leptons and contributions to $pp \to WW$ and $H \to WW$*, *JHEP* **02** (2016) 119 [arXiv:1509.04292] [INSPIRE].

[106] R. Dermisek, E. Lunghi and S. Shin, *New decay modes of heavy Higgs bosons in a two Higgs doublet model with vectorlike leptons*, arXiv:1512.07837 [INSPIRE].

[107] CMS collaboration, *Searches for new physics using the $t\bar{t}$ invariant mass distribution in pp collisions at $\sqrt{s} = 8$ TeV*, *Phys. Rev. Lett.* **111** (2013) 211804 [*Erratum ibid.* **112** (2014) 119903] [arXiv:1309.2030] [INSPIRE].

[108] ATLAS collaboration, *Search for new resonances in $W\gamma$ and $Z\gamma$ final states in pp collisions at $\sqrt{s} = 8$ TeV with the ATLAS detector*, *Phys. Lett.* **B 738** (2014) 428 [arXiv:1407.8150] [INSPIRE].

[109] CMS collaboration, *Search for neutral MSSM Higgs bosons decaying into a pair of bottom quarks*, *JHEP* **11** (2015) 071 [arXiv:1506.08329] [INSPIRE].

[110] ATLAS collaboration, *Search for neutral Higgs bosons of the minimal supersymmetric standard model in pp collisions at $\sqrt{s} = 8$ TeV with the ATLAS detector*, *JHEP* **11** (2014) 056 [arXiv:1409.6064] [INSPIRE].

[111] ATLAS collaboration, *Search for new phenomena in the dijet mass distribution using $p-p$ collision data at $\sqrt{s} = 8$ TeV with the ATLAS detector*, *Phys. Rev.* **D 91** (2015) 052007 [arXiv:1407.1376] [INSPIRE].

[112] K.G. Chetyrkin, J.H. Kuhn and M. Steinhauser, *RunDec: A Mathematica package for running and decoupling of the strong coupling and quark masses*, *Comput. Phys. Commun.* **133** (2000) 43 [hep-ph/0004189] [INSPIRE].

[113] J.M. Campbell, R.K. Ellis and C. Williams, *Vector boson pair production at the LHC*, *JHEP* **07** (2011) 018 [arXiv:1105.0020] [INSPIRE].

JHEP05(2016)009